


Influence of nuclear mass uncertainties on radiative neutron-capture ratesC. Ma (马畅)^{1,2}, Z. Li (李竹)³, Z. M. Niu (牛中明) ^{1,2,*} and H. Z. Liang (梁豪兆)^{4,5}¹*School of Physics and Materials Science, Anhui University, Hefei 230601, China*²*Institute of Physical Science and Information Technology, Anhui University, Hefei 230601, China*³*School of Physics and Nuclear Energy Engineering, Beihang University, Beijing 100191, China*⁴*RIKEN Nishina Center, Wako 351-0198, Japan*⁵*Department of Physics, Graduate School of Science, University of Tokyo, Tokyo 113-0033, Japan*

(Received 9 January 2019; revised manuscript received 8 July 2019; published 22 August 2019)

Neutron-capture rate plays a crucial role in the rapid neutron-capture process (r-process) and nuclear mass is one of the most important inputs for the estimations of neutron-capture rates. In this work, we employ ten nuclear mass models, including macroscopic, macroscopic-microscopic, and microscopic models, to calculate the radiative neutron-capture rates for the nuclei relevant to the r-process at various temperatures $T = 10^5$ – 10^{10} K. It is found that the differences in the predictions of neutron-capture rate using these mass models get larger when moving to the neutron-rich and superheavy regions, whereas they generally become smaller with the increase of temperature. Taking the nuclei on the $N = 126$ r-process path as examples, we find that the uncertainties of neutron-capture rates at $T = 10^9$ K range from about one to four orders of magnitude. The influence of the experimental mass errors on neutron-capture rates is investigated as well.

DOI: [10.1103/PhysRevC.100.024330](https://doi.org/10.1103/PhysRevC.100.024330)**I. INTRODUCTION**

The origin of heavy elements is one of the greatest unanswered questions in physics [1]. The rapid neutron-capture process (r-process) is responsible for about half of the solar abundances for the elements heavier than iron [2,3]. In the r-process, rapid neutrons are successively captured by the seed nuclei and hence produce many unstable nuclei, which then β decay to the next isotopic chains. By continuous neutron captures and β decays, the heavy elements are synthesized via the r-process. Therefore, the neutron-capture rates and β -decay half-lives play important roles in the r-process studies [4–10].

The measurements of β -decay half-lives have approached the r-process path around the $N = 82$ region [11]. In contrast, although great effort has been devoted to direct measurements of neutron-capture rates, for instance, $^{69}\text{Ni}(n, \gamma)^{70}\text{Ni}$ [12], they still mainly concentrate on the nuclei near the β -stability line [13]. Since the r-process involves thousands of different unstable neutron-rich nuclei, the theoretical predictions of neutron-capture rates are inevitable for understanding the r-process. At present, neutron-capture rates are usually calculated [14–17] via the Hauser-Feshbach statistical model [18]. Based on the Hauser-Feshbach statistical model, several code packages have been developed and used for the nucleosynthesis applications, such as the famous TALYS [19,20] and NON-SMOKER [14] code packages. They have been employed to calculate the thermonuclear reaction rates in the BRUSLIB [16] and REACLIB [17] databases.

The calculations of neutron-capture rates require a number of nuclear physics inputs, and nuclear mass is one of the

most important, which can significantly affect the predicted neutron-capture rates. Nowadays, two types of global nuclear mass models are widely used in the nuclear mass predictions: the macroscopic-microscopic and microscopic mass models [21]. Many macroscopic-microscopic mass models have been developed during recent years, such as the finite-range droplet model (FRDM) [22] and the Weizsäcker-Skyrme (WS) model [23]. This type of mass model is usually composed of macroscopic smooth parts and microscopic oscillating parts, and their accuracies are generally around 500 keV. The latest version of the WS model (WS4) achieved an accuracy of about 300 keV. On the other hand, the microscopic mass models are much more complicated and also need more computational time to calculate the masses of all nuclei on the nuclear chart. However, they are usually believed to be better with regard to extrapolation. In the relativistic framework, the relativistic mean-field (RMF) model [24–29] has been employed to systematic mass predictions of nuclei from proton-drip line to neutron-drip line by using the effective interaction TMA [30]. Recently, an effective interaction PC-PK1 was proposed [31], its root-mean-square (rms) deviation with respect to known masses is remarkably reduced to about 1 MeV [32,33], and the coupling between the bound states and the continuum due to the pairing correlations have been investigated systematically [34]. The microscopic nuclear mass models in the nonrelativistic framework also achieved great progress in recent years. A series of Skyrme Hartree-Fock-Bogoliubov (HFB) mass models have been developed, and their accuracies are about 600 keV [35–37], which are similar to the macroscopic-microscopic nuclear mass models.

These nuclear mass models generally predict similar nuclear masses in the known region, and their accuracies can be further improved by using the CLEAN image reconstruction

*zmnium@ahu.edu.cn

technique [38], the radial basis function approach [39–43], and neural network approach [44–47]. However, they can still give quite different nuclear mass predictions, which even exceed 10 MeV, for the nuclei far from the stability line [4]. The r-path nuclei are far from the stability line, so it is necessary to investigate the influence of nuclear mass uncertainties on neutron-capture rates. TALYS [19,20] is a publicly available code for simulation of nuclear reactions. This code includes many state-of-the-art nuclear models, in order to cover all main reaction mechanisms encountered in light particle-induced nuclear reactions, such as the direct, pre-equilibrium, and compound reaction mechanisms. It has been widely used to predict the radiative neutron-capture rates in the r-process simulations [48–51].

In this work, we will also employ the TALYS code to calculate the radiative neutron-capture rates of nuclei relevant to the r-process. The correlations between nuclear masses and r-process characteristics as well as sensitivity studies to individual nuclear masses have been discussed in recent works [51,52]. Instead of changing nuclear masses with the variations of ± 0.5 MeV [51], the mass differences among ten widely used nuclear models are regarded as the uncertainties of mass predictions in the unknown region and their impacts on the calculations of neutron-capture rates will be investigated in this work. In addition, the experimental errors of nuclear masses are also relatively large for those very neutron-rich nuclei, so their influence on the calculations of radiative neutron-capture rates will be investigated as well. These results of neutron-capture rates and the corresponding discussion are presented in Sec. III. In Sec. II, a brief introduction to the TALYS is given. The summary is given in Sec. IV.

II. TALYS CODE AND NUCLEAR REACTION MODELS

In TALYS, the Hauser-Feshbach statistical model is employed to estimate compound reactions. It assumes that the capture process occurs by means of the intermediary production of a compound nucleus which can reach a state of thermodynamic equilibrium [18]. Based on this statistical model, TALYS estimates the compound cross sections by summing all possible binary contributions, i.e.,

$$\begin{aligned} \sigma_{\alpha\alpha'}^{\mu} &= D_{\text{comp}} \pi \lambda^2 \sum_{J=\text{mod}(I^{\mu}+s,1)}^{I_{\text{max}}+I^{\mu}+s} \sum_{\Pi=-1}^1 \frac{2J+1}{(2I^{\mu}+1)(2s+1)} \\ &\times \sum_{j=|J-I^{\mu}|}^{J+I^{\mu}} \sum_{l=|j-s|}^{j+s} \sum_{j'=|J-I'|}^{J+I'} \sum_{l'=|j'-s'|}^{j'+s'} \delta_{\pi}(\alpha) \delta_{\pi}(\alpha') \\ &\times \frac{\mathcal{T}_{\alpha l j}^J(E_a) \mathcal{T}_{\alpha' l' j'}^J(E_{a'})}{\sum_{\alpha'', l'', j''} \delta_{\pi}(\alpha'') \mathcal{T}_{\alpha'' l'' j''}^J(E_{a''})} W_{\alpha l j \alpha' l' j'}^J. \end{aligned} \quad (1)$$

In the above expression, μ represents the energy level of the target nucleus. α is a channel designation of the initial system as $\alpha = \{a, s, E_a, E_x^{\mu}, I, \Pi_x\}$, where a , E_a , and E_x^{μ} denote the projectile type, the projectile energy, and the excitation energy of the target nucleus, respectively, while the quantities with a prime is for the final system. J and Π stand for the total angular momentum and parity of the compound nucleus. Besides, λ is the wavelength of relative motion, D_{comp} is the

normalized factor to exclude the direct and pre-equilibrium contributions, \mathcal{T} is the transmission coefficient derived by ECIS-06 [53], and W is the width fluctuation correction factor. $\delta_{\pi}(\alpha) = 1$ or 0 if the system obeys or violates the parity conservation. Clearly, the compound cross section can be derived out if the transmission coefficients of all possible reaction channels are known. According to the TALYS model [19,20,54], the variations in nuclear masses can change the optical potential depths and hence affect \mathcal{T} in Eq. (1), so the calculation of compound cross sections is highly correlated with the employed masses of relevant nuclei.

Since Eq. (1) supplies cross-section estimations as functions of projectile energies, the effective neutron-capture rates can be derived by Maxwell-Boltzmann averaging. Because the thermodynamic equilibrium mechanism works well at the stellar conditions, the Maxwell probability distribution for the relative energies E of the projectiles and seed nuclei are employed in the predictions. Furthermore, such conditions make the target nuclei range from their ground states to other excited states, whose relative populations obey the Boltzmann distribution. With the above considerations, the reaction rates at the temperature T can be averaged as

$$\begin{aligned} N_A \langle \sigma v \rangle_{\alpha\alpha'}^*(T) &= \left(\frac{8}{\pi m} \right)^{\frac{1}{2}} \frac{N_A}{(kT)^{\frac{3}{2}} G_I(T)} \sum_{\mu} \frac{2I^{\mu}+1}{2I^0+1} \\ &\times \int_0^{+\infty} \sigma_{\alpha\alpha'}^{\mu}(E) E \exp\left(-\frac{E+E_x^{\mu}}{kT}\right) dE, \end{aligned} \quad (2)$$

in which m denotes the reduced mass of the initial system, k is the Boltzmann constant, and N_A is the Avogadro number. $G_I(T)$ stands for T -dependent normalized partition function, i.e.,

$$G_I(T) = \sum_{\mu} (2I^{\mu}+1)/(2I^0+1) \exp(-E_x^{\mu}/kT). \quad (3)$$

Based on this premise, the effective stellar rate per pair of particles in the entrance channel can be calculated by the TALYS.

III. RESULTS AND DISCUSSION

In this section, we mainly discuss the deviations of neutron-capture rate predictions induced by the uncertainties of nuclear masses. The mass predictions of ten nuclear models are used in our calculations, including two microscopic (HFB-31 [37] and RMF [30]), five macroscopic-microscopic (FRDM12 [55], extended Thomas-Fermi plus Strutinsky integral ETFSI-2 [56] and ETFSI-Q [57], KTUY formula developed by H. Koura, T. Tachibana, M. Uno and M. Yamada [58], and WS4 [23]), one macroscopic (the Bethe-Weizsäcker formula BW2 [59]), and other two global mass models (the Bhagwat formula developed by A. Bhagwat [60] and the Duflo-Zuker formula DZ10 [61]). These ten theoretical models are only used in the mass-unknown region. Otherwise, the experimental masses from 2016 atomic mass evaluation (AME2016) [62,63] are adopted in the calculations. If there is no mass for the specific nucleus in one model, the evaluation

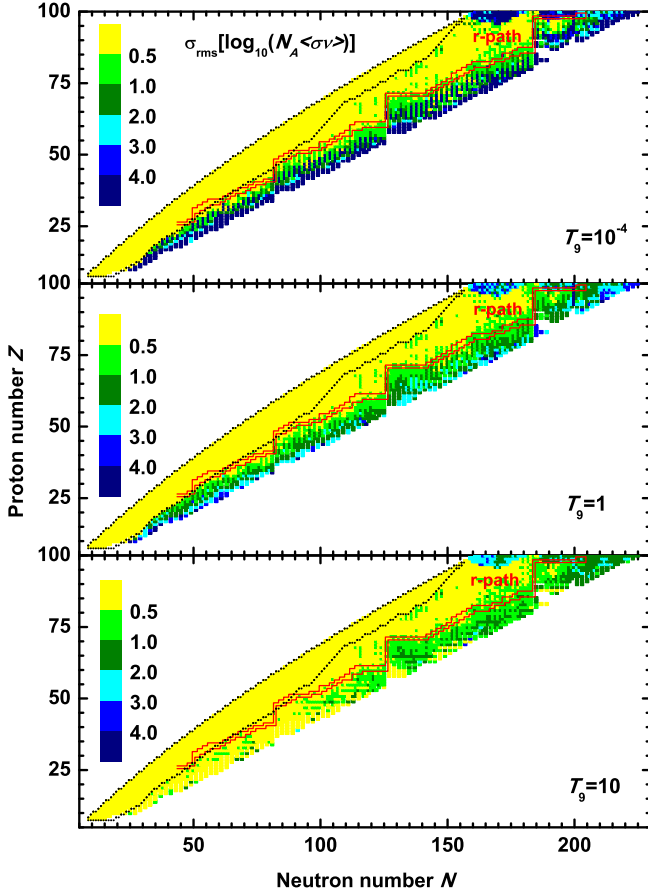


FIG. 1. Uncertainties of radiative neutron-capture rates from nuclear mass uncertainties at different temperatures. The boundaries of nuclei with known Q values in AME2016 are shown by the black contours. The r-process path from Ref. [7] is shown for guiding eyes, which is predicted based on the classical r-process model.

which is included as a subroutine in TALYS are performed. The combination of experimental and theoretical mass values may result in large discontinuities. To avoid this, when calculating quantities that depend on two masses of different origins (theory and experiment), the values derived from only the theoretical models are used, just like the method in Ref. [51]. The influence of experimental mass errors on the calculations is also investigated.

In this work, three sets of neutron-capture rates at different temperatures $T_9 = 10^{-4}$, 1, and 10 are calculated by TALYS. Here, T_9 denotes the astrophysical temperature in the unit of 10^9 K. The data tables for the neutron-capture rates are available as the Supplemental Material [64]. In order to quantify the uncertainties induced by differences of various nuclear mass models, at each temperature the root-mean-square (rms) deviations of the reaction rates σ_{rms} are calculated as

$$\sigma_{\text{rms}}(\log_{10} R) = \left[\frac{1}{n-1} \sum_{i=1}^n (\log_{10} R_i - \overline{\log_{10} R})^2 \right]^{1/2}, \quad (4)$$

where R denotes the calculated neutron-capture rate $N_A \langle \sigma v \rangle$ in the unit of $\text{mol}^{-1} \text{cm}^3 \text{s}^{-1}$. The subscript i is used to indicate

different mass models and $n = 10$ is the number of nuclear models used in this work.

Figure 1 shows overall distributions of $\sigma_{\text{rms}}(\log_{10} R)$ at three different temperatures in the neutron-rich region. For guiding eyes, the r-process path calculated based on the classical r-process model by using the RMF mass predictions is shown as well [7]. The classical r-process model [65] is a simplification of the dynamical r-process model, in which the waiting-point approximation is employed and the astrophysical conditions are usually determined by fitting to the solar r-process abundance distribution. Notice that the r-process paths in modern simulations may be different from that in Fig. 1; e.g., those in the neutron star merger environments are notably farther from stability than that in Fig. 1. Clearly, the deviations in the calculated neutron-capture rates are relatively larger for the exotic neutron-rich and superheavy nuclei. However, it is found that they are generally compressed as the temperature rises. Since the experimental masses will be used when available, $\sigma_{\text{rms}}(\log_{10} R)$ within the contour lines are exactly zero. We should also note that the radiative neutron-capture rates could reduce to very small values or even zero with the decrease of temperatures. These values would make $\sigma_{\text{rms}}(\log_{10} R)$ too large or even divergent and hence make these deviations unreliable. To deal with such cases, a threshold value for the reaction rates is introduced, which is set to $N_A \langle \sigma v \rangle_{\text{th}} = 10^{-15} \text{ mol}^{-1} \text{cm}^3 \text{s}^{-1}$ in this work. That is the reaction rates will be modified to $N_A \langle \sigma v \rangle_{\text{th}}$ when they are smaller than $N_A \langle \sigma v \rangle_{\text{th}}$. However, if all of the ten rates stay below $N_A \langle \sigma v \rangle_{\text{th}}$, the calculated deviation is also meaningless. So only those reactions whose rate predictions are larger than $N_A \langle \sigma v \rangle_{\text{th}}$ in at least four mass models are remained to get reasonable evaluations of $\sigma_{\text{rms}}(\log_{10} R)$.

To better study the change tendency of $\sigma_{\text{rms}}(\log_{10} R)$, we show the distribution of $\sigma_{\text{rms}}(\log_{10} R)$ with respect to the distance from the β -stability line $Z_\beta - Z$ at $T_9 = 1$ in Fig. 2. The average values of $\sigma_{\text{rms}}(\log_{10} R)$ with respect to $Z_\beta - Z$

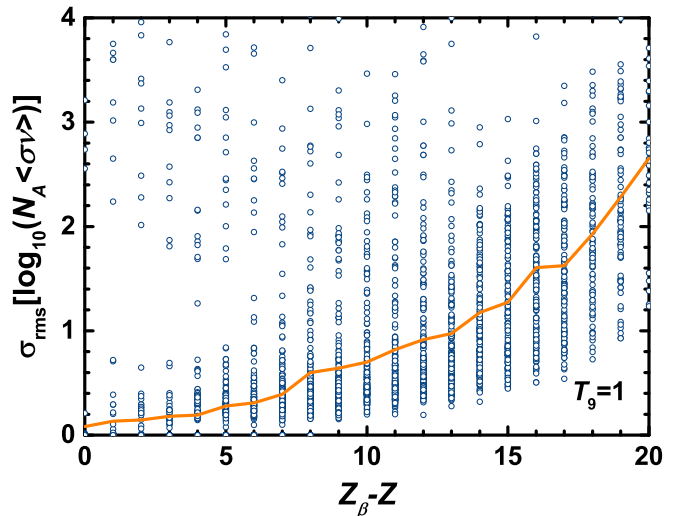


FIG. 2. Distribution of σ_{rms} with respect to the distance from the β -stability line $Z_\beta - Z$ at $T_9 = 1$, where Z_β is the proton number of nucleus on the β -stability line with a given mass number [41]. The average values of σ_{rms} are shown by the solid line.

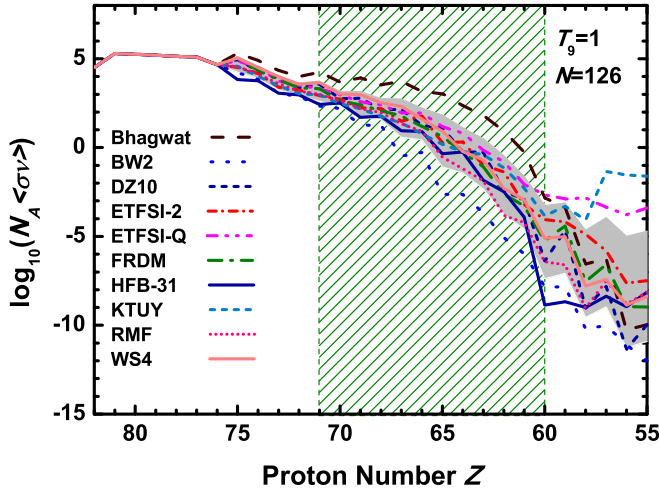


FIG. 3. Distributions of the radiative neutron-capture rates for $N = 126$ isotones at $T_9 = 1$ with different mass models. The gray band shows one standard deviations $\sigma_{\text{rms}}(\log_{10} R)$ from the average values for all mass models considered here. The r-process path from Ref. [7] is denoted by the hatched area, which is predicted based on the classical r-process model.

are also presented. In general, $\sigma_{\text{rms}}(\log_{10} R)$ gets larger as the reaction moves away from the β -stability line. This can be well understood since those nuclear mass models are generally well tuned with the known experimental data. When moving away from the β -stability line, the mass predic-

tions would become more unreliable, and differences between those models get larger. Taking ^{263}Bi as an example, its mass difference between HFB-31 and WS4 models can reach 16.45 MeV, and the resulting deviation in the reaction rates is $\Delta \log_{10}(N_A \langle \sigma v \rangle) = 3.75$.

To focus on the neutron-capture rates on the r-process path, we check the results of $N = 126$ isotones and show them in Fig. 3. When moving to the exotic neutron-rich region, the rates fall down by about 15 orders of magnitude (from about $10^5 \text{ mol}^{-1} \text{ cm}^3 \text{ s}^{-1}$ to about $10^{-10} \text{ mol}^{-1} \text{ cm}^3 \text{ s}^{-1}$). Since the experimental masses for $N = 126$ isotones only exist when the proton numbers of projectiles $Z \geq 76$, theoretical models are used when $Z = 75$ and drastic changes in neutron-capture rates are observed for Bhagwat and HFB-31 models, respectively. As we remove protons to $Z = 55$, the deviations in neutron-capture rates can increase to about five orders of magnitude. For the nuclei on the r-process path, the deviations increase from about one order of magnitude at $Z = 71$ to about four orders of magnitude at $Z = 60$. These deviations are generally more significant than those in Ref. [51], since the mass differences among these ten mass models are usually larger than 0.5 MeV when extrapolating to the mass-unknown region. This turns out that the systematic uncertainties of nuclear masses have strong impacts on the neutron-capture rates for the r-path nuclei and eventually can significantly affect the r-process abundances.

Apart from nuclear masses, neutron-capture rates are also sensitive to the astrophysical temperature [16,17,48], as shown in Fig. 1. To illustrate their temperature dependencies

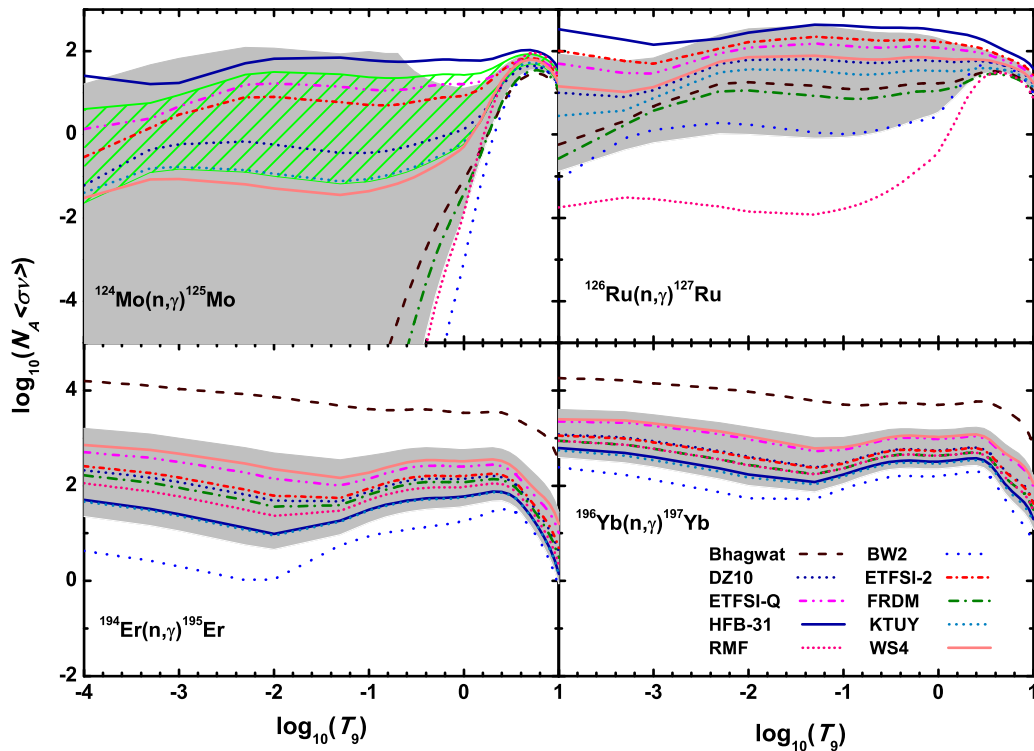


FIG. 4. Radiative neutron-capture rates of ^{124}Mo , ^{126}Ru , ^{194}Er , and ^{196}Yb as a function of temperature for various nuclear mass models. The gray bands show the deviations in neutron-capture rates, i.e., one standard deviations $\sigma_{\text{rms}}(\log_{10} R)$ among all the ten models, while the hatched area is the same but only for DZ10, ETFSI-2, ETFSI-Q, HFB-31, KTUY, and WS4 models.

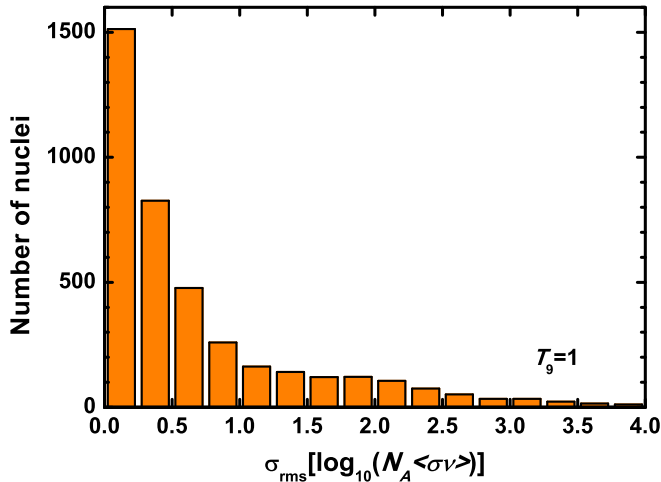


FIG. 5. Statistical histogram of numbers of nuclei within given ranges of $\sigma_{\text{rms}}(\log_{10} R)$ at $T_9 = 1$.

in detail, we give the results of ^{124}Mo and ^{126}Ru on the $N = 82$ r-process path as well as ^{194}Er and ^{196}Yb on the $N = 126$ r-process path in Fig. 4. The gray bands in Fig. 4 show the rms deviations $\sigma_{\text{rms}}(\log_{10} R)$, and they are generally reduced with the increase of the temperature. Notice that there are very large $\sigma_{\text{rms}}(\log_{10} R)$ for the case of $^{124}\text{Mo}(n, \gamma)^{125}\text{Mo}$ when $T_9 \lesssim 1$, which is clearly induced by the rapid decreases of the neutron-capture rates of ^{124}Mo when $T_9 \lesssim 1$ for the Bhagwat, BW2, FRDM, and RMF models. The predicted reaction energies of $^{124}\text{Mo}(n, \gamma)^{125}\text{Mo}$ for the Bhagwat, BW2, FRDM, and RMF models are -0.052 , -0.453 , -0.119 , and -0.237 MeV, respectively, which indicating the reactions are endergonic. As the temperature decreases, the reaction rates tend to zeros because of the constraints on conservation of energy. Therefore, the large $\sigma_{\text{rms}}(\log_{10} R)$ for $^{124}\text{Mo}(n, \gamma)^{125}\text{Mo}$ is an effect of approaching the neutron-drip line of single-neutron separation energy. The same effect could be seen wherever mass models disagree on the neutron number at which, moving along an isotopic chain, the one-neutron separation energies become negative. If we neglect these results from the calculations of $\sigma_{\text{rms}}(\log_{10} R)$, the $\sigma_{\text{rms}}(\log_{10} R)$ calculated by the remaining six models would be remarkably reduced, and the hatched areas in Fig. 4 show the corresponding results.

As an end of the discussion of $\sigma_{\text{rms}}(\log_{10} R)$, Fig. 5 gives the statistical histogram of the numbers of nuclei within given ranges of $\sigma_{\text{rms}}(\log_{10} R)$. For about 3000 (76.9%) nuclei the deviations of neutron-capture rates are within one order of magnitude, but it should be noticed that about 1400 (35.6%) nuclei with known masses contribute to this block. There are still a certain amount of nuclei with $\sigma_{\text{rms}}(\log_{10} R)$ between one and three orders of magnitude, i.e., 547 (13.7%) nuclei with $1 < \sigma_{\text{rms}}(\log_{10} R) \leq 2$ and 266 (6.6%) nuclei with $2 < \sigma_{\text{rms}}(\log_{10} R) \leq 3$.

Although experimental mass errors are generally too small to affect the calculations of neutron-capture rates, they could become non-negligible for those very neutron-rich nuclei. Taking Zr and Sb isotopes as examples, the influence of

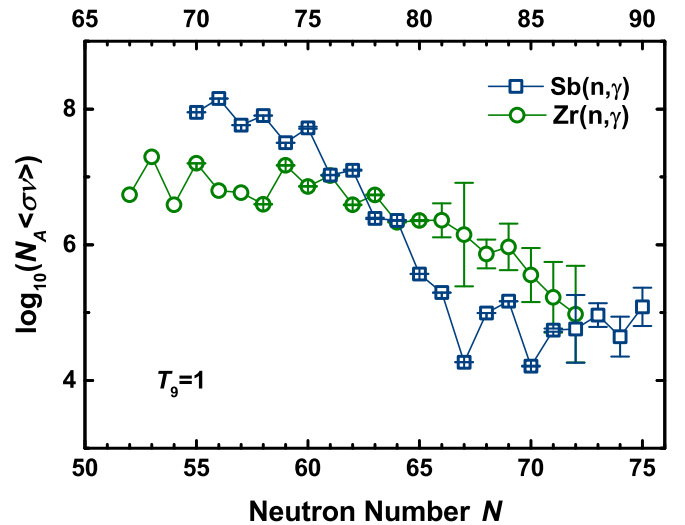


FIG. 6. Neutron-capture rates of Zr and Sb isotopes and their corresponding uncertainties from experimental mass errors at $T_9 = 1$. The lower horizontal axis denotes the neutron number of Zr isotopes, while the upper one is for Sb isotopes. The experimental data are taken from AME2016.

experimental mass errors is studied, and we show the results in Fig. 6. The calculated rates and their errors of neutron-capture rates in Fig. 6 are evaluated with the Monte Carlo method, in which 500 rates for each (n, γ) process are calculated based on the random sampling of nuclear masses within their uncertainties. It can be seen from the figure that the deviations in neutron-capture rates can reach one order of magnitude, which cannot be neglected, for those nuclei located on the neutron-rich boundary of the known region. Taking ^{138}Sb and ^{107}Zr as examples, their experimental mass errors are 1.064 and 1.122 MeV, respectively, and their deviations in the logarithm of neutron-capture rates can reach 0.50 and 0.76. This indicates that not only theoretical mass predictions but also the precisions of experimental masses need to be improved to give more reliable predictions for neutron-capture rates.

IV. SUMMARY AND CONCLUSION

In this study, a comprehensive evaluation of the deviations in radiative neutron-capture rates among different nuclear models and their temperature dependencies have been performed by TALYS. The mass differences among various theoretical models have been taken as the embodiments of uncertainties of mass predictions in the unknown region, and we have studied their influences on the predictions of neutron-capture rates within the temperatures ranging from 10^5 to 10^{10} K. When $T = 10^9$ K, the deviations in neutron-capture rates are within one order of magnitude for most nuclei, and they become larger when moving to the very neutron-rich and superheavy region. Taking $N = 126$ isotones as examples, the deviations in neutron-capture rates that located at the r-process path increase from about one to about four orders of magnitude. The temperature dependence discussion shows

that the rise of the temperature may compress the differences in the rate predictions. Apart from the impact of theoretical uncertainties, the influence of experimental mass errors can also result in nearly one order of magnitude deviations for those neutron-rich isotopes located on the boundary of the known region. Therefore, both reliable global mass model and accurate experimental mass values are crucial to the r-process studies.

ACKNOWLEDGMENTS

This work was partly supported by the National Natural Science Foundation of China under Grants No. 11875070 and No. 11711540016, the Natural Science Foundation of Anhui Province under Grant No. 1708085QA10, and the Open Fund for Discipline Construction, Institute of Physical Science and Information Technology, Anhui University.

-
- [1] E. Haseltin, *Discover* **23**, 37 (2002).
- [2] E. M. Burbidge, G. R. Burbidge, W. A. Fowler, and F. Hoyle, *Rev. Mod. Phys.* **29**, 547 (1957).
- [3] F.-K. Thielemann, M. Eichler, I. V. Panov, and B. Wehmeyer, *Annu. Rev. Nucl. Part. Sci.* **67**, 253 (2017).
- [4] M. R. Mumpower, R. Surman, G. C. McLaughlin, and A. Aprahamian, *Prog. Part. Nucl. Phys.* **86**, 86 (2016).
- [5] B. Sun, F. Montes, L. S. Geng, H. Geissel, Y. A. Litvinov, and J. Meng, *Phys. Rev. C* **78**, 025806 (2008).
- [6] Z. M. Niu, B. Sun, and J. Meng, *Phys. Rev. C* **80**, 065806 (2009).
- [7] Z. M. Niu, Y. F. Niu, H. Z. Liang, W. H. Long, T. Nikšić, D. Vretenar, and J. Meng, *Phys. Lett. B* **723**, 172 (2013).
- [8] Z. M. Niu, H. Z. Liang, B. H. Sun, W. H. Long, and Y. F. Niu, *Phys. Rev. C* **99**, 064307 (2019).
- [9] X. D. Xu, B. Sun, Z. M. Niu, Z. Li, Y. Z. Qian, and J. Meng, *Phys. Rev. C* **87**, 015805 (2013).
- [10] Z. Li, Z. M. Niu, B. H. Sun, N. Wang, and J. Meng, *Acta Phys. Sin.* **61**, 072601 (2012).
- [11] G. Audi, F. G. Kondev, M. Wang, W. J. Huang, and S. Naimi, *Chin. Phys. C* **41**, 030001 (2017).
- [12] S. N. Liddick, A. Spyrou, B. P. Crider, F. Naqvi, A. C. Larsen, M. Guttormsen, M. Mumpower, R. Surman, G. Perdikkakis, D. L. Bleuel *et al.*, *Phys. Rev. Lett.* **116**, 242502 (2016).
- [13] NucRates, National Nuclear Data Center [<http://www.nndc.bnl.gov/astro/>]
- [14] T. Rauscher and F.-K. Thielemann, *At. Data Nucl. Data Tables* **75**, 1 (2000).
- [15] M. Beard, E. Uberseder, R. Crowter, and M. Wiescher, *Phys. Rev. C* **90**, 034619 (2014).
- [16] The Brussels Nuclear Library for Astrophysics Applications, maintained by Institut d'Astronomie et d'Astrophysique, Université Libre de Bruxelles [<http://www.astro.ulb.ac.be/bruslib>].
- [17] R. H. Cyburt, A. M. Amthor, R. Ferguson, Z. Meisel, K. Smith, S. Warren, A. Heger, R. D. Hoffman, T. Rauscher, A. Sakharuk *et al.*, *Astrophys. J. Suppl.* **189**, 240 (2010).
- [18] W. Hauser and H. Feshbach, *Phys. Rev.* **87**, 366 (1952).
- [19] A. J. Koning, S. Hilaire, and M. C. Duijvestijn, in *Proceedings of the International Conference on Nuclear Data for Science and Technology, April 22–27, 2007, Nice, France*, edited by O. Bersillon, F. Gunsing, E. Bauge, R. Jacqmin, and S. Leray (EDP Sciences, Nice, France, 2008), pp. 211–214.
- [20] A. J. Koning and D. Rochman, *Nucl. Data Sheets* **113**, 2841 (2012).
- [21] D. Lunney, J. M. Pearson, and C. Thibault, *Rev. Mod. Phys.* **75**, 1021 (2003).
- [22] P. Möller, J. R. Nix, W. D. Myers, and W. J. Swiateck, *At. Data Nucl. Data Tables* **59**, 185 (1995).
- [23] N. Wang, M. Liu, X. Z. Wu, and J. Meng, *Phys. Lett. B* **734**, 215 (2014).
- [24] J. Meng, H. Toki, S. G. Zhou, S. Q. Zhang, W. H. Long, and L. S. Geng, *Prog. Part. Nucl. Phys.* **57**, 470 (2006).
- [25] D. Vretenar, A. V. Afanasjev, G. A. Lalazissis, and P. Ring, *Phys. Rep.* **409**, 101 (2005).
- [26] H. Z. Liang, J. Meng, and S. G. Zhou, *Phys. Rep.* **570**, 1 (2015).
- [27] Z. M. Niu, Y. F. Niu, Q. Liu, H. Z. Liang, and J. Y. Guo, *Phys. Rev. C* **87**, 051303(R) (2013).
- [28] Z. M. Niu, Y. F. Niu, H. Z. Liang, W. H. Long, and J. Meng, *Phys. Rev. C* **95**, 044301 (2017).
- [29] P. Jiang, Z. M. Niu, Y. F. Niu, and W. H. Long, *Phys. Rev. C* **98**, 064323 (2018).
- [30] L. S. Geng, H. Toki, and J. Meng, *Prog. Theor. Phys.* **113**, 785 (2005).
- [31] P. W. Zhao, Z. P. Li, J. M. Yao, and J. Meng, *Phys. Rev. C* **82**, 054319 (2010).
- [32] X. M. Hua, T. H. Heng, Z. M. Niu, B. H. Sun, and J. Y. Guo, *Sci. China: Phys. Mech. Astron.* **55**, 2414 (2012).
- [33] Q. S. Zhang, Z. M. Niu, Z. P. Li, J. M. Yao, and J. Meng, *Front. Phys.* **9**, 529 (2014).
- [34] X. W. Xia, Y. Lim, P. W. Zhao, H. Z. Liang, X. Y. Qu, Y. Chen, H. Liu, L. F. Zhang, S. Q. Zhang, Y. Kim *et al.*, *At. Data Nucl. Data Tables* **121–122**, 1 (2018).
- [35] S. Goriely, N. Chamel, and J. M. Pearson, *Phys. Rev. Lett.* **102**, 152503 (2009).
- [36] S. Goriely, S. Hilaire, M. Girod, and S. Péru, *Phys. Rev. Lett.* **102**, 242501 (2009).
- [37] S. Goriely, N. Chamel, and J. M. Pearson, *Phys. Rev. C* **93**, 034337 (2016).
- [38] Irving O. Morales, P. Van Isacker, V. Velazquez, J. Barea, J. Mendoza-Temis, J. C. López Vieyra, J. G. Hirsch, and A. Frank, *Phys. Rev. C* **81**, 024304 (2010).
- [39] N. Wang and M. Liu, *Phys. Rev. C* **84**, 051303(R) (2011).
- [40] Z. M. Niu, Z. L. Zhu, Y. F. Niu, B. H. Sun, T. H. Heng, and J. Y. Guo, *Phys. Rev. C* **88**, 024325 (2013).
- [41] J. S. Zheng, N. Y. Wang, Z. Y. Wang, Z. M. Niu, Y. F. Niu, and B. Sun, *Phys. Rev. C* **90**, 014303 (2014).
- [42] Z. M. Niu, B. H. Sun, H. Z. Liang, Y. F. Niu, and J. Y. Guo, *Phys. Rev. C* **94**, 054315 (2016).
- [43] Z. M. Niu, H. Z. Liang, B. H. Sun, Y. F. Niu, J. Y. Guo, and J. Meng, *Sci. Bull.* **63**, 759 (2018).
- [44] R. Utama, J. Piekarewicz, and H. B. Prosper, *Phys. Rev. C* **93**, 014311 (2016).
- [45] Z. M. Niu and H. Z. Liang, *Phys. Lett. B* **778**, 48 (2018).
- [46] L. Neufcourt, Y. C. Cao, W. Nazarewicz, and F. Viens, *Phys. Rev. C* **98**, 034318 (2018).
- [47] H. F. Zhang, L. H. Wang, J. P. Yin, P. H. Chen, and H. F. Zhang, *J. Phys. G: Nucl. Part. Phys.* **44**, 045110 (2017).

- [48] S. Goriely, S. Hilaire, and A. J. Koning, *Astron. Astrophys.* **487**, 767 (2008).
- [49] D. Martin, A. Arcones, W. Nazarewicz, and E. Olsen, *Phys. Rev. Lett.* **116**, 121101 (2016).
- [50] S. Goriely, S. Hilaire, S. Péru, and K. Sieja, *Phys. Rev. C* **98**, 014327 (2018).
- [51] M. R. Mumpower, R. Surman, D.-L. Fang, M. Beard, P. Möller, T. Kawano, and A. Aprahamian, *Phys. Rev. C* **92**, 035807 (2015).
- [52] M. R. Mumpower, G. C. McLaughlin, R. Surman, and A. W. Steiner, *J. Phys. G: Nucl. Part. Phys.* **44**, 034003 (2017).
- [53] J. Raynal, CEA Saclay Report No. CEA-N-2772, 1994 (unpublished).
- [54] A. J. Koning and J. P. Delaroche, *Nucl. Phys. A* **713**, 231 (2003).
- [55] P. Möller, W. D. Myers, H. Sagawa, and S. Yoshida, *Phys. Rev. Lett.* **108**, 052501 (2012).
- [56] S. Goriely, Capture Gamma-Ray Spectroscopy and Related Topics: 10th International Symposium, AIP Conf. Proc. No. 529 (AIP, New York, 2000), p. 287.
- [57] J. M. Pearson, R. C. Nayak, and S. Goriely, *Phys. Lett. B* **387**, 455 (1996).
- [58] H. Koura, T. Tachibana, M. Uno, and M. Yamada, *Prog. Theor. Phys.* **113**, 305 (2005).
- [59] M. W. Kirson, *Nucl. Phys. A* **798**, 29 (2008).
- [60] A. Bhagwat, *Phys. Rev. C* **90**, 064306 (2014).
- [61] J. Duflo and A. P. Zuker, *Phys. Rev. C* **52**, R23 (1995).
- [62] W. J. Huang, G. Audi, M. Wang, F. G. Kondev, S. Naimi, and X. Xu, *Chin. Phys. C* **41**, 030002 (2017).
- [63] M. Wang, G. Audi, F. G. Kondev, W. J. Huang, S. Naimi, and X. Xu, *Chin. Phys. C* **41**, 030003 (2017).
- [64] See Supplemental Material at <http://link.aps.org/supplemental/10.1103/PhysRevC.100.024330> for the data tables of neutron-capture rates.
- [65] B. Pfeiffer, K.-L. Kratz, and F.-K. Thielemann, *Z. Phys. A* **357**, 235 (1997).